Impact of Noise Level on the Accuracy of Automated Measurement of CT Number Linearity on ACR CT and Computational Phantoms

Choirul Anam (PhD)[1]*, Riska Amilia (BSc)[1], Ariij Naufal (MSc)[1], Heri Sutanto (PhD)[1], Yanurita Dwihapsari (MSc)[2], Toshioh Fujibuchi (PhD)[3], Geoff Dougherty (PhD)[4]

[1]Department of Physics, Faculty of Sciences and Mathematics, Diponegoro University, Jl. Prof Soedarto, SH Tembalang, Semarang 50275, Central Java, Indonesia
[2]Department of Physics, Faculty of Science and Data Analytics, Institute Teknologi Sepuluh Nopember, Kampus ITS Sukolilo – Surabaya 60111, East Java, Indonesia
[3]Department of Health Sciences, Faculty of Medical Sciences, Kyushu University, 3-1-1 Maidashi, Higashi-ku, Fukuoka 812-8582, Japan
[4]Department of Applied Physics and Medical Imaging, California State University Channel Islands, Camarillo, CA 93012, USA

ABSTRACT

Background: Methods for segmentation, i.e., Full-segmentation (FS) and Segmentation-rotation (SR), are proposed for maintaining Computed Tomography (CT) number linearity. However, their effectiveness has not yet been tested against noise.

Objective: This study aimed to evaluate the influence of noise on the accuracy of CT number linearity of the FS and SR methods on American College of Radiology (ACR) CT and computational phantoms.

Material and Methods: This experimental study utilized two phantoms, ACR CT and computational phantoms. An ACR CT phantom was scanned by a 128-slice CT scanner with various tube currents from 80 to 200 mA to acquire various noises, with other constant parameters. The computational phantom was added by different Gaussian noises between 20 and 120 Hounsfield Units (HU). The CT number linearity was measured by the FS and SR methods, and the accuracy of CT number linearity was computed on two phantoms.

Results: The two methods successfully segmented both phantoms at low noise, i.e., less than 60 HU. However, segmentation and measurement of CT number linearity are not accurate on a computational phantom using the FS method for more than 60-HU noise. The SR method is still accurate up to 120 HU of noise.

Conclusion: The SR method outperformed the FS method to measure the CT number linearity due to its endurance in extreme noise.

Citation: Anam Ch, Amilia R, Naufal A, Sutanto H, Dwihapsari Y, Fujibuchi T, Dougherty G. Impact of Noise Level on the Accuracy of Automated Measurement of CT Number Linearity on ACR CT and Computational Phantoms. *J Biomed Phys Eng*. 2023;13(4):353-362. doi: 10.31661/jbpe.v0i0.2302-1599.

Keywords

ACR CT Phantom; Computational Phantom; Diagnostic Imaging; Image Quality Enhancement; Noise; CT Number Linearity; Computed Tomography Scanner; Quality of Health Care

*Corresponding author: Choirul Anam
Department of Physics, Faculty of Sciences and Mathematics, Diponegoro University, Jl. Prof Soedarto, SH Tembalang, Semarang 50275, Central Java, Indonesia
E-mail: anam@fisika.fsm.undip.ac.id

Received: 21 February 2023
Accepted: 15 May 2023

Introduction

Quantitative Computed Tomography (QCT) has transformed into a main pillar for patient diagnosis and early detection of various diseases, such as anemia, lung cancer, and osteoporosis [1-5]. QCT largely relies on the CT number presented in the Hounsfield Units (HU) [6-7], and its accuracy becomes a paramount aspect to avoid the

occurrence of misdiagnosis [8-10].

However, the accuracy of CT number measurement might be disrupted by the presence of noise [11], defined as an undesirable fluctuation of CT numbers in images due to the imperfection of the CT system [12-14]. However, the presence of noise is evitable in the CT image [15]. The noise can lead to inaccuracies in CT number measurements [16] and a decline in the visibility of low-contrast objects [17-18]. Accordingly, noise potentially diminishes the primary objective of the diagnostic image [19-22].

CT number linearity is one of the important parameters to obtain and maintain the accuracy of CT number and manually tested by plotting the mean CT number of each material available within the phantom versus their densities [23-25].

A study was conducted on the measurement of automatic CT number linearity [26], which is highly dependent on the accuracy of the segmentation of objects with different CT numbers. Two methods of segmentation are used, as follows: 1) the Full-segmentation (FS) method, done by segmenting all objects one by one [27] with a high probability for segmentation errors, especially for objects with CT numbers close to backgrounds (0 HU). Moreover, segmenting all objects one by one also requires a relatively long computation time [28]. Recently, an improved method based on Segmentation-rotation (SR) technique is proposed [26], which is only performed on one object with a large different CT number from the background. After segmenting an object, other objects are segmented with a template matching, namely by rotating the centre of the object to a center of the phantom with certain angles. However, the efficacy of the two methods against noise has not been investigated. This study aimed to evaluate the influence of noise on the accuracy of CT number linearity in two methods (FS and SR methods) on American College of Radiology (ACR) CT and the computational phantoms.

Material and Methods

American College of Radiology (ACR) Computed Tomography (CT) phantom

This experimental study utilized an ACR CT 464 phantom (Gammex Inc, USA), including four modules for measuring many image quality parameters. CT number linearity was measured on the first module, including five objects with different densities: polyethylene, bone-equivalent, air, acrylic, and solid water. The phantom was scanned by a 128-slice CT scanner (GE Revolution Evo, GE Healthcare, Waukesha, Wisconsin) with a tube voltage of 120 kV, slice thickness of 1.25 mm, pitch of 0.53, Field of View (FOV) of 235 mm, revolution time of 0.8 s, and various tube currents: 80, 100,120, 140, 160, and 200 mA. Tube currents were varied to obtain different image noise levels. The schematic of the ACR CT phantom is depicted in Figure 1.

Computational phantom

Scans were done many times from very low to very high tube currents to find many noise levels, which were from very low to very high. Computational multi-pin phantoms were developed to simplify this task without real scans. This multi-pin computational phantom is considered the first module of the ACR CT phantom. The positions of the multi-pin for the vertical line are tabulated in Table 1. However, the computational phantoms had a slight difference from the real ACR CT phantom, i.e., there were no wire ramps for measuring slice thickness in the computational phantoms. The wire ramps are not needed since the CT number linearity is measured in the current study.

The computational phantom has developed as follows: 1) the software constructed a phantom with pixel size 512×512 and a radius of 200 mm (as the ACR CT phantom). The phantom (as background) had a pixel value of 0 HU (mimicking the solid water), while the air surrounding had a pixel value of -1000 HU (mimicking the air) and 2) a point of radius 60 mm

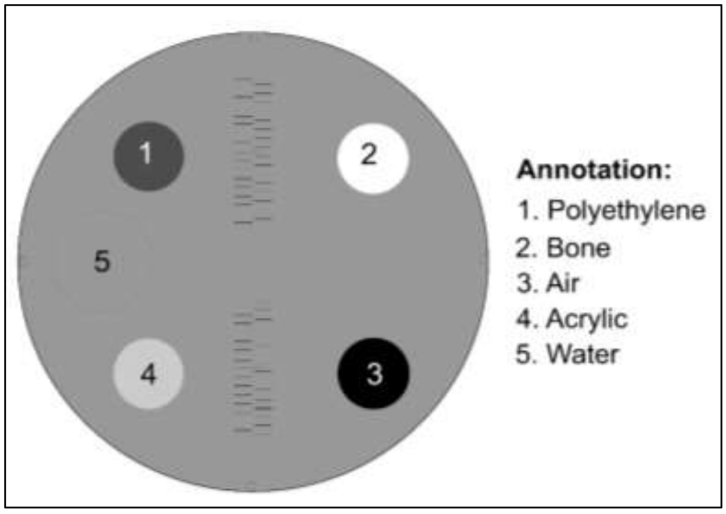

Figure 1: The schematic of the American College of Radiology (ACR) Computed Tomography (CT) phantom.

Table 1: The rotation angle and specific Computed Tomography (CT) number of each pin number (material).

Pin number	Angle (°)	Material	Computed tomography (CT) number (HU)
1	135	Polyethylene	-94
2	45	Bone-equivalent	955
3	-45	Air	-1000
4	225	Acrylic	120
Background	-	Solid water	0

from centre was determined and rotated with certain angles to acquire the coordinates of four objects. From each material, a disk kernel with a radius of 13 mm was designed and filled with the specific CT number.

In this stage, the multi-pin image was produced, but it was not a real image. Therefore, the blurring process was conducted, by convoluting the image with Point Spread Function (PSF (x, y)). The PSF was set with an SD value of 1 pixel and operated with Equation 1 to degrade the spatial resolution of image ($I(x, y)$) with the value of k, obtained by equation (2).

$$I(x,y)=\frac{1}{k}\left[P(x,y)\otimes PSF(x,y)\right] \quad (1)$$

$$k=\sum\sum PSF(x,y) \quad (2)$$

After the blurring process, Gaussian noise was added to the phantom with a specific Standard Deviation (SD). Finally, a degraded image with blurring and noise was yielded. This study varied noises, including 20, 40, 60, 80, 100, and 120 HU to observe the ability and accuracy of two methods in measuring CT number linearity. The multi-pin computational phantoms were integrated into in-house software. The multi-pin computational phantoms were integrated into IndoQCT software (Diponegoro University, Semarang Indonesia, https://indosect.com/indoqct/).

Methods for CT number linearity measurement

This study evaluated the influence of noise variation on measuring CT number linearity by two methods, i.e., FS and SR methods. The FS method segmented four materials (bone equivalent, polyethylene, acrylic, and air) with specified thresholds (Table 2), followed by the determination of the centre of each material. After that, the rotation of 45° was conducted to acquire the coordinate of water with the phantom's coordinate as the rotary axis with polyethylene. The FS method was shown in Figure 2.

In contrast, the SR method was conducted by thresholding the phantom and only bone insert at first, determining their centres, and rotating both coordinates with specific angles to acquire the other coordinates (90° for air, 180° for acrylic, -90° for polyethylene, and -135° for water) [26].

The further steps for both methods are such as creating the ROI for each material, plotting the linearity graph of CT number vs densities, and computing the R^2.

Results

American College of Radiology (ACR) Computed Tomography (CT) phantom

Figure 3 depicts the relationship of variation in tube current with measured noise. As expected, increasing the tube current led to

Table 2: Thresholding value of full-segmentation (FS) method

Object	Threshold value (HU)	
	Bottom limit	Upper limit
Polyethylene	-120	-70
Bone-equivalent	750	1300
Air	-	-800
Acrylic	100	150

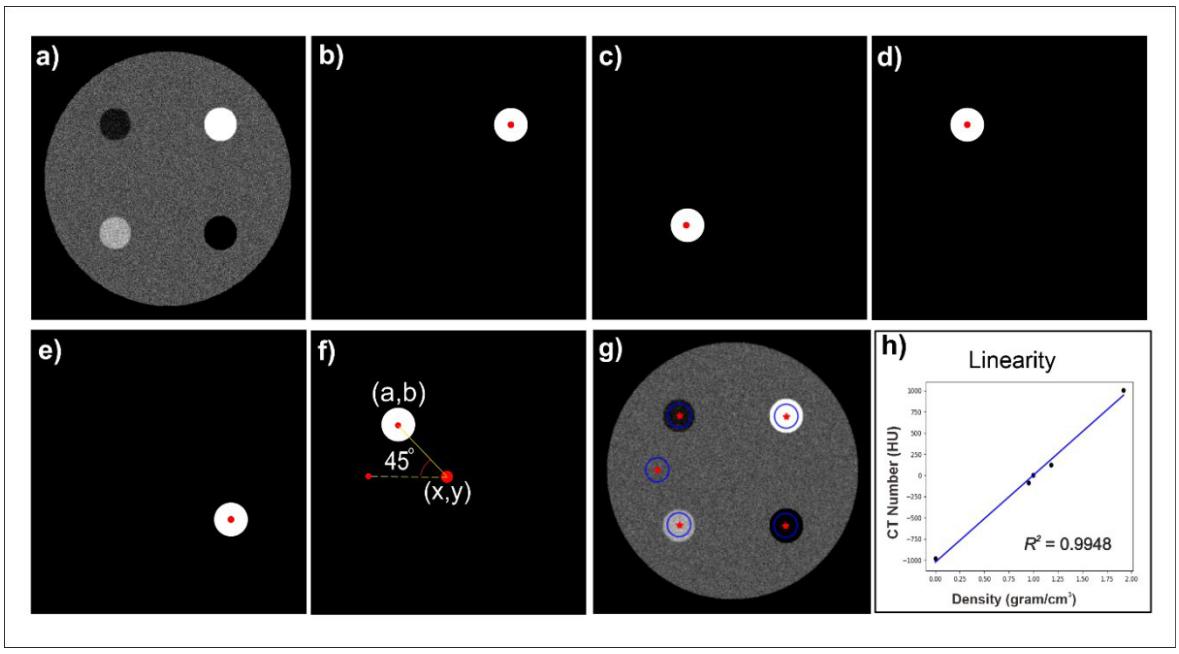

Figure 2: The measurement steps of computed tomography number linearity with full segmentation method. a) original image of the computational phantom, b) segmenting the bone, c) segmenting the acrylic, d) segmenting the polyethylene, e) segmenting the air, f) rotating the phantom and polyethylene centroid to acquire the water coordinates, g) creating the region of interest (ROI) for each material, h) yielding the CT number linearity graph.

decreasing noise. At tube currents of 160 and 200 mA, the difference in noise is ignorable. However, the noise at 200 mA than 160 mA is slightly larger because it is a random event in this study.

Segmentation results of ACR CT phantom with 2.01 HU by SR and FS methods are depicted in Figure 4. Further, the segmentations with both methods were accurate, even at the highest noise level. The results of measuring CT number linearity in ACR CT phantom are tabulated in Table 3. Increasing the tube current yielded similar results from both methods (P-value>0.05). The CT number linearities passed the tolerance level for all measured noise levels from both methods (R^2>0.99).

Computational phantom

The segmentation results of the computational phantom for a noise level of 120 HU

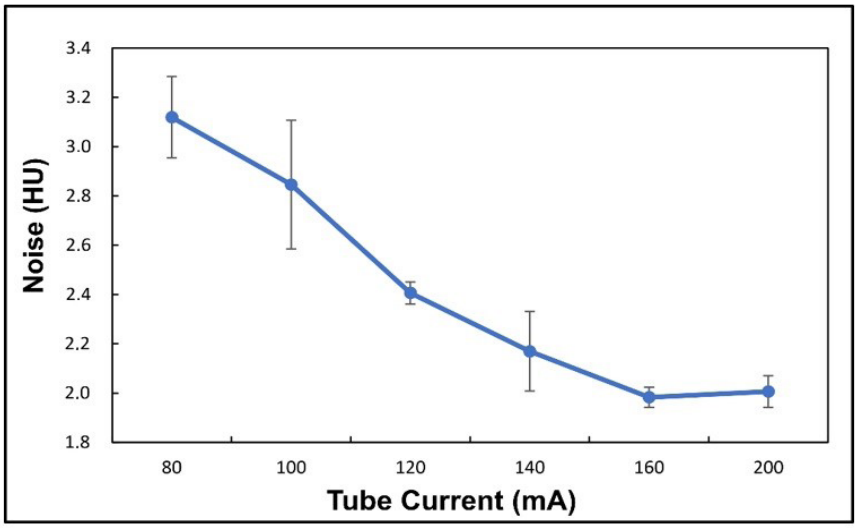

Figure 3: The graph of the correlation between tube current and image noise.

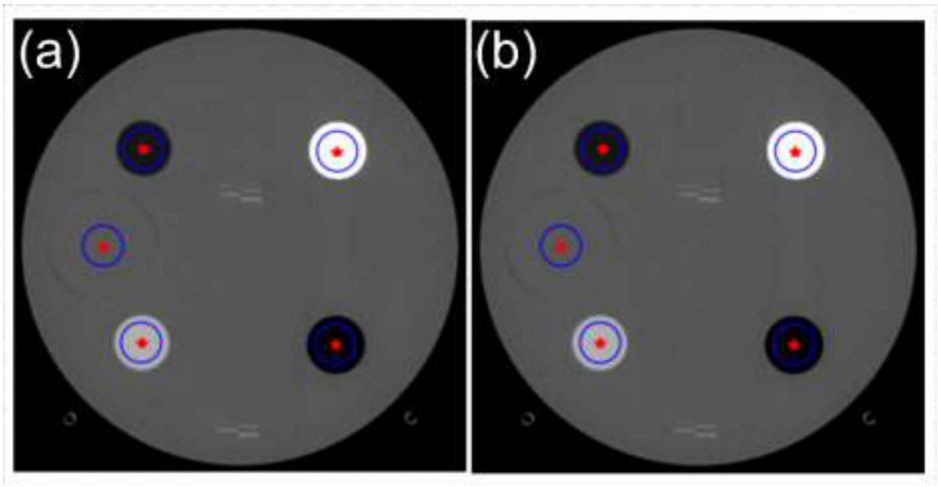

Figure 4: The results of segmentation on the American College of Radiology (ACR) Computed Tomography (CT) phantom with noise level 2.01 HU by (a) full-segmentation method and (b) segmentation-rotation method.

with both methods are depicted in Figure 5, meanwhile, those of CT number linearity measurement with various noise levels are tabulated in Table 4, showing the accuracy of the FS method largely depends on the noise level. At a noise of 60 HU and more, the FS method failed to segment polyethylene and acrylic objects. At the higher noise, the segmentation results are different from the two objects. As a consequence, the CT numbers of the two measured objects are different from the expected values (Table 4). At high noise levels, the CT

Table 3: The result of measured Computed Tomography (CT) number of five objects within the American College of Radiology (ACR) CT phantom with various noise levels

Material	Method	Noise (HU)					
		3.13±0.17	**2.85±0.26**	**2.41±0.05**	**2.17±0.16**	**1.98±0.04**	**2.01±0.06**
Polyethylene	Full-Segmentation	-90.5	-90.4	-90.3	-90	-90.3	-89.9
	Segmentation-Rotation	-90.5	-90.4	-90.3	-90	-90.3	-89.8
Bone-equivalent	Full-Segmentation	1004.7	1005.6	1002.1	1006.1	1006.6	1006.7
	Segmentation-Rotation	1004.7	1005.6	1002.1	1006.1	1006.6	1006.7
Air	Full-Segmentation	-984.2	-984.1	-982.5	-984.9	-984.9	-985.2
	Segmentation-Rotation	-984.2	-984.1	-982.5	-984.9	-984.9	-985.2
Acrylic	Full-Segmentation	126.2	125.9	125.2	126	126.1	125.9
	Segmentation-Rotation	126.2	125.8	125.2	126	126.1	125.9
Solid water	Full-Segmentation	2.7	3	3.1	3	3.2	3.3
	Segmentation-Rotation	2.7	3	3.1	3	3.2	3.3
R^2	Full-Segmentation	0.9948	0.9947	0.9948	0.9948	0.9948	0.9948
	Segmentation-Rotation	0.9948	0.9947	0.9948	0.9948	0.9948	0.9948

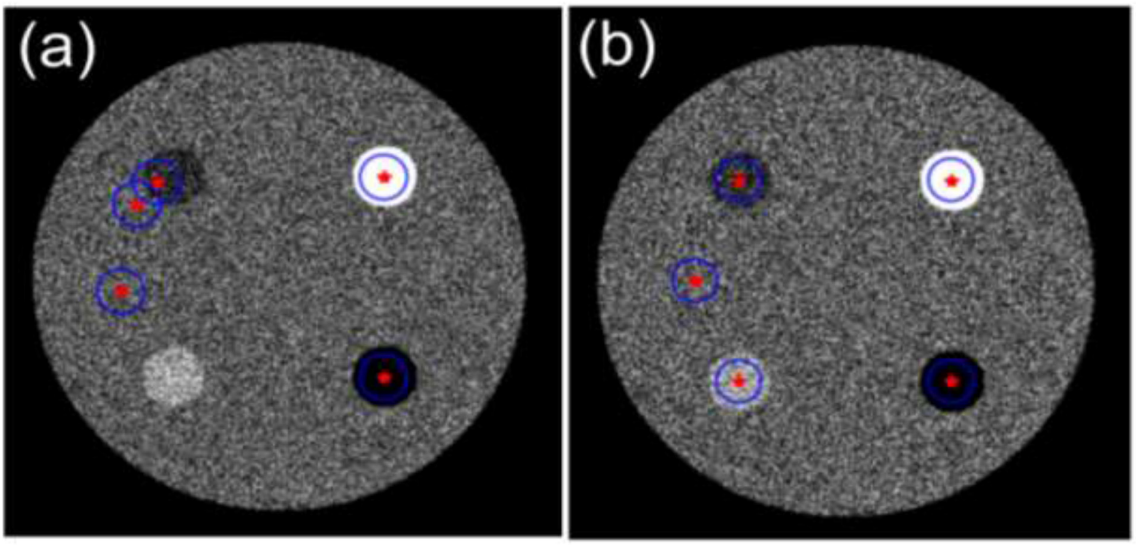

Figure 5: The results of segmentation on the computational phantom with the noise level of 120 HU by (a) full-segmentation method and (b) segmentation method.

Table 4: The result of computational phantom measurement with various noises.

Material	Method	Noise (HU)					
		20	40	60	80	100	120
Polyethylene	Full-Segmentation	-93.5	-95	-70.3	-88.6	-54.6	-64.2
	Segmentation-Rotation	-93.6	-95	-94	-96.2	-82.5	-86.7
Bone-equivalent	Full-Segmentation	954.2	954.7	952.8	955.8	952.1	949.3
	Segmentation-Rotation	954.2	954.7	953.3	955.7	950	949.3
Air	Full-Segmentation	-998.1	-998.2	-999.5	-998.6	-994.7	-985.2
	Segmentation-Rotation	-998.3	-998.2	-997.9	-998.4	-995	-990.8
Acrylic	Full-Segmentation	118.7	119.4	122.8	79.7	85.1	-1.1
	Segmentation-Rotation	118.3	119.4	121.4	118.3	113.3	111.5
Solid water	Full-Segmentation	-0.6	0.5	-1.0	-3.1	0.4	-6.8
	Segmentation-Rotation	-0.8	0.5	-1.4	-5.8	-0.4	0.5
R^2	Full-Segmentation	0.9971	0.9971	0.9979	0.9945	0.9951	0.9846
	Segmentation-Rotation	0.9971	0.997	0.9972	0.997	0.9971	0.9967

number linearity of the FS method failed to meet the standard value (R^2<0.99); however, the SR method produced segmentations that were more resistant to noise. Even at noise levels up to 120 HU, the segmentations produced by the SR method remained highly accurate. Consequently, the CT number and CT number linearity values are still accurate up to that noise level.

Methods had similar linearity values for noise levels less than 60 HU (Table 4). However, the linearity results of the two methods differed significantly, with a *P*-value>0.05 for higher noise levels (greater than 60 HU).

Discussion

Image noise, as an undesirable image parameter, leads to the degrading of the quality of CT images [29]. The accurate diagnosis is affected by the noise due to the change in CT number. The most frequent method, widely used to measure CT number linearity is FS; however, the SR method is proposed to overcome the limitations of the FS method.

The SR method outperformed the FS technique to measure the CT number linearity due to its rapidity and endurance in the extreme noise since it segments only for a material (i.e., bone equivalent) with large different CT numbers from the background, whilst the other objects were determined by the template based on the centre coordinate of phantom and bone equivalent [26]. As a result, the SR method is more resistant to higher noise levels, and the segmentation with the SR method is quickly performed and the CT number's linearity is accurately computed.

The FS method segments the four objects one by one, requiring more time than the SR method. Additionally, the CT numbers of acrylic and polyethylene are relatively similar to those of the background material. As a result, the segmentation of objects is difficult in high noise levels above 60 HU.

Nevertheless, the CT noise in clinical examination is usually not extreme [30], a diagnostic image generally contains lower noise, less than 10 HU. Therefore, measuring CT number linearity by both methods remains accurate since the error of the FS method just appeared with the noise of more than 60 HU. In this study, various noise levels were obtained from

different tube currents with other constant input parameters. The different tube current was selected because tube current variation had no significant effect on the produced CT number. Birnabum et al. [31] showed that the variation of tube current did not cause considerable changes in the CT number. Afifi et al. [32] also presented that varying tube currents had a minimum impact on CT number fluctuations.

Noise is an essential parameter in the CT image quality [12, 27], and its suppression in QCT is used to enhance the accuracy of diagnosis [33-35]. Cruz-Bastida et al. [36] reported that noise reduction in two phantoms (head and Catphan phantoms) significantly declines CT number bias, resulting in improving CT number accuracy. Therefore, testing CT number linearity routinely is important for establishing the accuracy of CT numbers for accurate diagnosis [37, 38].

The current study has two limitations, as follows: 1) the noise was only considered over a limited range of tube currents, with different results at a larger range of mA and 2) a computational phantom was used instead of real images of the ACR CT phantom for high noise levels up to 120 HU, in which the noise did not represent the actual noise generated by images reconstructed by Filtered Back-Projection, Iterative Reconstruction, or Deep Learning Reconstruction methods. Therefore, the effect of real high noise on the accuracy of object segmentation should be investigated in future studies in terms of CT number linearity. The noise characterization was based only on the noise level, not on the noise texture. Further, different noise textures will likely impact the segmentation accuracy of the FS and SR methods.

Conclusion

The SR method outperforms the FS method to measure the CT number linearity due to its endurance in extreme noise. Segmentation of objects and measurement of CT number linearity on ACR CT phantom using the FS method is only accurate when the noise is less than 60 HU, while the SR method is still accurate up to 120 HU of noise.

Authors' Contribution

Ch. Anam designed the project. R. Amilia, H. Sutanto, Y. Dwihapsari, and T. Fujibuchi performed the experiments. A. Naufal and Ch. Anam made the computational phantom. R. Amilia, Y. Dwihapsari, and G. Dougherty wrote the manuscript. All the authors read, modified, and approved the final version of the manuscript.

Ethical Approval

The research was approved by the Institutional Ethical Committee of Diponegoro University.

Funding

This work was funded by the World Class Research University (WCRU), Diponegoro University, No. 118-08/UN7.6.1/PP/2021.

Conflict of Interest

None

References

1. Li Y, Jiang Y, Yu X, Ren B, Wang C, Chen S, et al. Deep-learning image reconstruction for image quality evaluation and accurate bone mineral density measurement on quantitative CT: A phantom-patient study. *Front Endocrinol.* 2022;**13**:884306. doi: 10.3389/fendo.2022.884306. PubMed PMID: 36034436. PubMed PMCID: PMC9403270.
2. Barros MC, Altmayer S, Carvalho AR, Rodrigues R, Zanon M, Mohammed TL, et al. Quantitative computed tomography: What clinical questions can it answer in chronic lung disease? *Lung.* 2022;**200**(4):447-55. doi: 10.1007/s00408-022-00550-1. PubMed PMID: 35751660. PubMed PMCID: PMC9378468.2.
3. Shin SY, Hong IK, Jo YS. Quantitative computed tomography texture analysis: can it improve diagnostic accuracy to differentiate malignant lymph nodes? *Cancer Imaging.* 2019;**19**(1):25. doi: 10.1186/s40644-019-0214-8. PubMed PMID: 31113494. PubMed PMCID: PMC6530003.
4. Pocock N. Use of dual energy X-ray absorptiometry,

the trabecular bone score and quantitative computed tomography in the evaluation of chronic kidney disease-mineral and bone disorders. *Nephrology.* 2017;**2**:19-21. doi: 10.1111/nep.13016. PubMed PMID: 28429557.

5. Yoo JS, Chung SH, Lim MC, Kim YJ, Kim KG, Hwang JH, Kim YH. Computed tomography-based quantitative assessment of lower extremity lymphedema following treatment for gynecologic cancer. *J Gynecol Oncol.* 2017;**28**(2):18. doi: 10.3802/jgo.2017.28.e18. PubMed PMID: 28028991. PubMed PMCID: PMC5323285.
6. Al-Hayek Y, Spuur K, Davidson R, Hayre C, Zheng X. The impacts of vertical off-centring, localiser direction, phantom positioning and tube voltage on CT number accuracy: An experimental study. *J Imaging.* 2022;**8**(7):175. doi: 10.3390/jimaging8070175. PubMed PMID: 35877619. PubMed PMCID: PMC9316438.
7. Zhang R, Cruz-Bastida JP, Gomez-Cardona D, Hayes JW, Li K, Chen GH. Quantitative accuracy of CT numbers: Theoretical analyses and experimental studies. *Med Phys.* 2018;**45**(10):4519-28. doi: 10.1002/mp.13119. PubMed PMID: 30102414. PubMed PMCID: PMC7301593.
8. Booz C, Noeske J, Albrecht MH, Lenga L, Martin SS, Yel I, et al. Diagnostic accuracy of quantitative dual-energy CT-based bone mineral density assessment in comparison to Hounsfield unit measurements using dual x-ray absorptiometry as standard of reference. *Eur J Radiol.* 2020;**132**:109321. doi: 10.1016/j.ejrad.2020.109321. PubMed PMID: 33017775.
9. Ahern DP, McDonnell JM, Riffault M, Evans S, Wagner SC, Vaccaro AR, et al. A meta-analysis of the diagnostic accuracy of Hounsfield units on computed topography relative to dual-energy X-ray absorptiometry for the diagnosis of osteoporosis in the spine surgery population. *Spine J.* 2021;**21**(10):1738-49. doi: 10.1016/j.spinee.2021.03.008. PubMed PMID: 33722727.
10. Buenger F, Eckardt N, Sakr Y, Senft C, Schwarz F. Correlation of bone density values of quantitative computed tomography and Hounsfield units measured in native computed tomography in 902 vertebral bodies. *World Neurosurg.* 2021;**151**:599-606. doi: 10.1016/j.wneu.2021.04.093. PubMed PMID: 33933695.
11. Anam C, Triadyaksa P, Naufal A, Arifin Z, Muhlisin Z, Setiawati E, Budi WS. Impact of ROI size on the accuracy of noise measurement in CT on computational and ACR phantoms. *J Biomed Phys Eng.* 2022;**12**(4):359-68. doi: 10.31661/jbpe.v0i0.2202-1457. PubMed PMID: 36059282. PubMed PMCID: PMC9395624.
12. Zarb F, Rainford L, McEntee MF. Image quality assessment tools for optimization of CT images. *Radiography.* 2010;**16**(2):147-53. doi: 10.1016/j.radi.2009.10.002.
13. Diwakar M, Kumar M. A review on CT image noise and its denoising. *Biomed Sig Processing and Control.* 2018;**42**:73-88. doi: 10.1016/j.bspc.2018.01.010.
14. Wisselink HJ, Pelgrim GJ, Rook M, Dudurych I, Van Den Berge M, De Bock GH, Vliegenthart R. Improved precision of noise estimation in CT with a volume-based approach. *Eur Radiol Exp.* 2021;**5**(1):39. doi: 10.1186/s41747-021-00237-x. PubMed PMID: 34505172. PubMed PMCID: PMC8429536.
15. Higaki T, Nakamura Y, Zhou J, Yu Z, Nemoto T, Tatsugami F, Awai K. Deep learning reconstruction at CT: Phantom study of the image characteristics. *Acad Radiol.* 2020;**27**(1):82-7. doi: 10.1016/j.acra.2019.09.008. PubMed PMID: 31818389.
16. Kanamori H, Nakamori N, Inoue K, Takenaka E. Effects of scattered X-rays on CT images. *Phys Med Biol.* 1985;**30**(3):239-49. doi: 10.1088/0031-9155/30/3/004. PubMed PMID: 3983234.
17. Zhang Y, Salehjahromi M, Yu H. Tensor decomposition and non-local means based spectral CT image denoising. *J Xray Sci Technol.* 2019;**27**(3):397-416. doi: 10.3233/XST-180413. PubMed PMID: 31081796. PMCID: PMC7371001.
18. Clark TJ, Hsu LD, Hippe D, Cowan S, Carnell J, Wang CL. Evaluation of diagnostic accuracy: multidetector CT image noise correction improves specificity of a Gaussian model-based algorithm used for characterization of incidental adrenal nodules. *Abdom Radiol.* 2019;**44**(3):1033-43. doi: 10.1007/s00261-018-1871-y. PubMed PMID: 30600378.
19. Sprawls P. AAPM tutorial CT image detail and noise. *Radiographics.* 1992;**12**(5):1041-6. doi: 10.1148/radiographics.12.5.1529128. PubMed PMID: 1529128.
20. Juluru K, Shih JC, Raj A, Comunale JP, Delaney H, Greenberg ED, et al. Effects of increased image noise on image quality and quantitative interpretation in brain CT perfusion. *Am J Neuroradiol.* 2013;**34**(8):1506-12. doi: 10.3174/ajnr.A3448. PubMed PMID: 23557960. PubMed PMCID: PMC4108445.
21. Madani A, Keyzer C, Gevenois PA. Quantitative computed tomography assessment of lung structure and function in pulmonary emphysema. *Eur Respir J.* 2001;**18**(4):720-30. doi: 10.1183/09031936.01.00255701. PubMed PMID:

11716178.

22. Lynch DA. Quantitative computed tomography of diffuse lung disease. *J Thorac Imaging*. 2013;**28**(5):264-5. doi: 10.1097/RTI.0b013e3182a14fd8. PubMed PMID: 23966091.
23. Li Y, Jiang Y, Liu H, Yu X, Chen S, Ma D, Gao J, Wu Y. A phantom study comparing low-dose CT physical image quality from five different CT scanners. *Quant Imaging Med Surg*. 2022;**12**(1):766-80. doi: 10.21037/qims-21-245. PubMed PMID: 34993117. PubMed PMCID: PMC8666789.
24. Mehnati P, Jafari TM, Ghavami M. CT Role in the assessment of existence of breast cancerous cells. *J Biomed Phys Eng*. 2020;**10**(3):349-56. doi: 10.31661/jbpe.v0i0.384. PubMed PMID: 32637379. PubMed PMCID: PMC7321400.
25. Lascola KM, O'Brien RT, Wilkins PA, Clark-Price SC, Hartman SK, Mitchell MA. Qualitative and quantitative interpretation of computed tomography of the lungs in healthy neonatal foals. *Am J Vet Res.* 2013;**74**(9):1239-46. doi: 10.2460/ajvr.74.9.1239. PubMed PMID: 23977897.
26. Anam C, Amilia R, Naufal A, Budi WS, Maya AT, Dougherty G. The automated measurement of CT number linearity using an ACR accreditation phantom. *Biomed Phys Eng Express.* 2022;**9**(1):017002. doi: 10.1088/2057-1976/aca9d5. PubMed PMID: 36541467.
27. Suyudi I, Anam C, Sutanto H, Triadyaksa P, Fujibuchi T. Comparisons of Hounsfield Unit Linearity between Images Reconstructed using an Adaptive Iterative Dose Reduction (AIDR) and a Filter Back-Projection (FBP) Techniques. *J Biomed Phys Eng*. 2020;**10**(2):215-24. doi: 10.31661/jbpe.v0i0.1912-1013. PubMed PMID: 32337189. PubMed PMCID: PMC7166214.
28. Anam C, Haryanto F, Widita R, Arif I, Dougherty G. Automated calculation of water-equivalent diameter (Dw) based on AAPM Task Group 220. *J Appl Clin Med Phys*. 2016;**17**(4):320-33. doi: 10.1120/jacmp.v17i4.6171. PubMed PMID: 27455491. PubMed PMCID: PMC5690059.
29. Anam C, Sutanto H, Adi K, Budi WS, Muhlisin Z, Haryanto F, et al. Development of a computational phantom for validation of automated noise measurement in CT images. *Biomed Phys Eng Express.* 2020;**6**(6):065001. doi: 10.1088/2057-1976/abb2f8. PubMed PMID: 35135906.
30. Anam C, Budi WS, Adi K, Sutanto H, Haryanto F, Ali MH, Fujibuchi T, Dougherty G. Assessment of patient dose and noise level of clinical CT images: automated measurements. *J Radiol Prot.* 2019;**39**(3):783-93. doi: 10.1088/1361-6498/ab23cc. PubMed PMID: 31117064.
31. Birnbaum BA, Hindman N, Lee J, Babb JS. Multidetector row CT attenuation measurements: assessment of intra- and interscanner variability with an anthropomorphic body CT phantom. *Radiology*. 2007;**242**(1):109-19. doi: 10.1148/radiol.2421052066. PubMed PMID: 17185663.
32. Afifi MB, Abdelrazek A, Deiab NA, Abd El-Hafez AI, El-Farrash AH. The effects of CT x-ray tube voltage and current variations on the relative electron density (RED) and CT number conversion curves. *J Radiat Res Appl Sci.* 2020;**13**(1):1-11. doi: 10.1080/16878507.2019.1693176.
33. Naidich DP, Marshall CH, Gribbin C, Arams RS, McCauley DI. Low-dose CT of the lungs: preliminary observations. *Radiology*. 1990;**175**(3):729-31. doi: 10.1148/radiology.175.3.2343122. PubMed PMID: 2343122.
34. Tanaka C, Ueguchi T, Shimosegawa E, Sasaki N, Johkoh T, Nakamura H, Hatazawa J. Effect of CT acquisition parameters in the detection of subtle hypoattenuation in acute cerebral infarction: a phantom study. *Am J Neuroradiol*. 2006;**27**(1):40-5. PubMed PMID: 16418353. PubMed PMCID: PMC7976079.
35. Einstein SA, Rong XJ, Jensen CT, Liu X. Quantification and homogenization of image noise between two CT scanner models. *J Appl Clin Med Phys*. 2020;**21**(1):174-78. doi: 10.1002/acm2.12798. PubMed PMID: 31859454. PubMed PMCID: PMC6964752.
36. Cruz-Bastida JP, Zhang R, Gomez-Cardona D, Hayes J, Li K, Chen GH. Impact of noise reduction schemes on quantitative accuracy of CT numbers. *Med Phys.* 2019;**46**(7):3013-24. doi: 10.1002/mp.13549. PMID: 31004439.
37. Kim JH, Chang Y, Ra JB. Denoising of polychromatic CT images based on their own noise properties. *Med Phys.* 2016;**43**(5):2251. doi: 10.1118/1.4945022. PubMed PMID: 27147337.
38. Christe A, Heverhagen J, Ozdoba C, Weisstanner C, Ulzheimer S, Ebner L. CT dose and image quality in the last three scanner generations. *World J Radiol.* 2013;**5**(11):421-9. doi: 10.4329/wjr.v5.i11.421. PubMed PMID: 24349646. PubMed PMCID: PMC3856334.